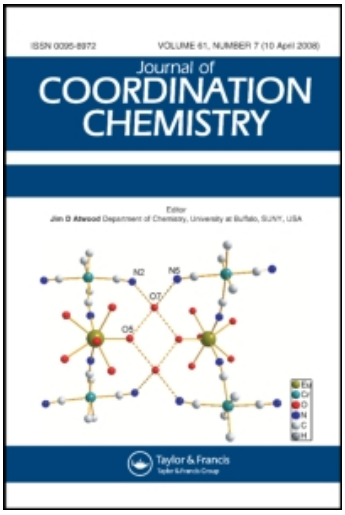

Journal of Coordination Chemistry
Publication details, including instructions for authors and subscription information:
http://www.informaworld.com/smpp/title~content=t713455674

Synthesis and characterization of vanadium(III) and vanadium(IV) polymers containing 3,5-pyrazoledicarboxylato

Hui Chen[a]; Chengbing Ma[a]; Shengchang Xiang[a]; Mingqiang Hu[a]; Youtao Si[a]; Changneng Chen[a]; Qiutian Liu[a]
[a] State Key Laboratory of Structural Chemistry, Fujian Institute of Research on the Structure of Matter, Fuzhou, Fujian 350002, China

To cite this Article Chen, Hui , Ma, Chengbing , Xiang, Shengchang , Hu, Mingqiang , Si, Youtao , Chen, Changneng and Liu, Qiutian(2008) 'Synthesis and characterization of vanadium(III) and vanadium(IV) polymers containing 3,5-pyrazoledicarboxylato', Journal of Coordination Chemistry, 61: 22, 3556 — 3567
To link to this Article: DOI: 10.1080/00958970802108825
URL: http://dx.doi.org/10.1080/00958970802108825

Journal of Coordination Chemistry
Vol. 61, No. 22, 20 November 2008, 3556–3567

Synthesis and characterization of vanadium(III) and vanadium(IV) polymers containing 3,5-pyrazoledicarboxylato

HUI CHEN, CHENGBING MA, SHENGCHANG XIANG, MINGQIANG HU, YOUTAO SI, CHANGNENG CHEN* and QIUTIAN LIU

State Key Laboratory of Structural Chemistry, Fujian Institute of Research on the Structure of Matter, Chinese Academy of Sciences, Fuzhou, Fujian 350002, China

(*Received 3 December 2007; in final form 13 February 2008*)

Three vanadium polymers $[V_2(\mu\text{-}OH)_2(H_2O)_2(Hpdc)_2]_n$ (**1**), $\{[Na_2(\mu\text{-}H_2O)_2][V_2O_2(pdc)_2]\}_n$ (**2**) and $\{[K_2(\mu\text{-}H_2O)][V_2O_2(pdc)_2]\}_n$ (**3**) ($H_3pdc = 3,5$-pyrazoledicarboxylate acid) have been hydrothermally synthesized and characterized by spectroscopic methods, magnetic susceptibility measurements and X-ray crystallography. The structure of **1** consists of infinite double-stranded chains. Both **2** and **3** are 3D coordination polymers, featuring ladder-like moieties, made up of $[V_2O_2(pdc)_2]$ subunits, interconnected by pairs of alkali ion chains. Variable-temperature magnetic behavior reveals the existence of antiferromagnetic interactions in **1** and dominant ferromagnetic interactions in **2** and **3**.

Keywords: Vanadium; Polymer; Synthesis; Characterization; Magnetism

1. Introduction

Metal-organic coordination polymers have drawn considerable interest due to their fascinating structures and potential applications in magnetism [1], catalysis [2, 3], molecular separation [4, 5] and other fields [6, 7]. A wide variety of network topologies have been constructed through different coordination geometries of the metal ions and the selection or design of multifunctional ligands. 3,5-Pyrazoledicarboxylic acid, which contains both O and N donors, can coordinate to metal ions to generate a variety of architectures [8–15]; only one dinuclear V(IV) complex has been reported [10]. With the diverse oxidation states and coordination chemistry of vanadium, we set out to prepare V/H_3pdc complexes and here report the synthesis and characterization of three vanadium polymers $[V_2(\mu\text{-}OH)_2(H_2O)_2(Hpdc)_2]_n$ (**1**), $\{[Na_2(\mu\text{-}H_2O)_2][V_2O_2(pdc)_2]\}_n$ (**2**) and $\{[K_2(\mu\text{-}H_2O)][V_2O_2(pdc)_2]\}_n$ (**3**).

*Corresponding author. Email: ccn@fjirsm.ac.cn

Journal of Coordination Chemistry
ISSN 0095-8972 print/ISSN 1029-0389 online © 2008 Taylor & Francis
DOI: 10.1080/00958970802108825

2. Experimental

2.1. *Materials and physical measurements*

All manipulations were performed under aerobic conditions. All reagents are commercially available analytical reagent grade and were used without further purification. Water was distilled before used as solvent. Elemental analyses were carried out on a Vario EL III Elemental Analyzer. IR spectra were recorded on a Magna-75 FT-IR spectrometer using KBr pellets in the range 4000–400 cm^{-1}. X-band EPR spectra were recorded on a Bruker-ER420 spectrometer at both room temperature and liquid nitrogen temperature for solid complexes. Variable-temperature magnetic susceptibilities were measured on a model CF-1 superconducting magnetometer in the temperature range 2–300 K with crystalline sample being kept in a capsule. Diamagnetic corrections were made with Pascal's constants for all the constituent atoms of the complex.

2.2. *Synthesis of the complexes*

A mixture of H_3pdc (1 mmol), VCl_3 (1 mmol) and $K_2C_2O_4$ (1.5 mmol) in 10 mL H_2O was sealed in a 25 mL Teflon-lined stainless steel autoclave and heated at 170°C for three days. Small dark crystals of **1** were recovered by filtration in 46% yield (0.112 g). Anal. Calcd for $C_{10}H_{10}N_4O_{12}V_2$ (%): C, 25.02; H, 2.10; N, 11.67. Found: C, 24.91; H, 2.43; N, 11.36. IR (KBr, cm^{-1}): 3196(s), 1650(s), 1552(m), 1497(m), 1431(m), 1347(s), 1313(m), 1226(m), 1026(m), 1009(m), 859(m), 780(m).

Reaction of H_3pdc (1 mmol), $VO(acac)_2$ (0.5 mmol) and NaOH (2 mmol) in 10 mL H_2O using the method described above gave red needle-like microcrystals of **2** in 32% yield (0.042 g). Anal. Calcd for $C_{10}H_6N_4Na_2O_{12}V_2$ (%): C, 23.01; H, 1.16; N, 10.73. Found: C, 23.17; H, 1.47; N, 10.77. IR (KBr, cm^{-1}): 3606(w), 3407(w), 3132(w), 1694(s), 1668(s), 1609(m), 1490(w), 1386(m), 1308(m), 1273(m), 1217(m), 1019(m), 902(s), 856(m), 777(m).

Reaction of H_3pdc (1 mmol), $VO(acac)_2$ (0.5 mmol), KOH (2 mmol) in 10 mL H_2O using the method described above gave red needle-like microcrystals of **3** in 38% yield (0.050 g). Anal. Calcd for $C_{10}H_4N_4K_2O_{11}V_2$ (%): C, 22.40; H, 0.75; N, 10.45. Found: C, 22.33; H, 0.69; N, 10.54. IR (KBr, cm^{-1}): 3616(w), 3130(m), 1651(s), 1621(m), 1486(w), 1381(m), 1320(m), 1275(m), 1224(m), 1020(m), 918(s), 859(m), 783(m).

2.3. *X-ray crystallography*

The X-ray single-crystal data were collected on a Saturn 70 CCD diffractometer for **1**, a Mercury CCD diffractometer for **2** and a Smart CCD diffractometer for **3**. The structures were solved by direct methods and refined by full matrix least-squares techniques using SHELXTL-97 [16]. All non-hydrogen atoms were refined anisotropically. Hydrogen atoms were determined with difference Fourier maps or geometrical calculations riding on the related atoms, and their positions and thermal parameters were fixed during the

Table 1. Crystallographic data and data collection parameters for **1**, **2** and **3**.

	1	**2**	**3**
Empirical formula	$C_{10}H_{10}N_4O_{12}V_2$	$C_{10}H_6N_4Na_2O_{12}V_2$	$C_{10}H_4K_2N_4O_{11}V_2$
Crystal size (mm^3)	$0.07 \times 0.05 \times 0.02$	$0.15 \times 0.06 \times 0.05$	$0.28 \times 0.10 \times 0.05$
Crystal system	Triclinic	Monoclinic	Monoclinic
Space group	$P\bar{1}$	$C2/c$	$P2/c$
Unit cell dimensions (Å, °)			
a	6.691(3)	23.232(14)	10.6609(4)
b	6.902(3)	3.788(2)	3.91240(10)
c	8.597(4)	20.064(12)	19.77410(10)
α	93.995(7)	90	90
β	101.040(3)	117.531(7)	104.965(2)
γ	109.259(5)	90	90
V(Å^3)	364.1(3)	1565.9(16)	796.80(4)
Z	1	4	2
Formula weight	480.10	522.05	536.25
Wavelength (Å)	0.71073	0.71073	0.71073
Temperature (K)	293(2)	293(2)	293(2)
D_{Calcd} ($Mg\,m^{-3}$)	2.190	2.214	2.235
Absorption coefficient (mm^{-1})	1.370	1.333	1.770
Parameter/restraints/data (obs.)	136/0/1373	144/5/1547	135/0/1203
θ range (°)	3.16–27.45	3.54–27.48	1.98–25.72
Reflections collected	2913	5591	4106
Independent reflections/R_{int}	1653/0.0213	1779/0.0272	1508/0.0477
R_1/wR_2 [$I > 2\sigma(I)$]	0.0288/0.0651	0.0314/0.0784	0.0563/0.1442
R_1/wR_2 (all)	0.0386/0.0691	0.0395/0.0835	0.0793/0.1610
Goodness-of-fit on F^2	1.029	1.010	1.144
Largest difference peak ($e\,Å^{-3}$)	0.376, −0.354	0.403, −0.325	0.524, −1.023

structure refinement. Selected crystallographic data and refinement details are displayed in table 1. Selected bond lengths and angles are listed in tables 2, 3 and 4 for **1**, **2** and **3**.

3. Results and discussion

3.1. *Syntheses and infrared spectra*

All complexes are air stable and insoluble in common solvents. Hydrothermal reaction of H_3pdc, VCl_3 and $K_2C_2O_4$ yielded little black crystals of **1**. Replacement of $K_2C_2O_4$ by other bases, such as NaOH or pyridine, didn't give **1**. V^{3+} is easily oxidized by O_2 and $K_2C_2O_4$ may prevent oxidation of V^{3+}. Changing the molar ratio of H_3pdc, VCl_3 and $K_2C_2O_4$ to 1 : 1 : 1 or 1 : 1 : 2 afforded the same product in comparable yields (varied from 36% to 58%). After reaction, the pH value of the solution is acidic, about 1.5 for 1 : 1 : 1, 2.0 for 1 : 1 : 1.5 and 2.5 for 1 : 1 : 2. The acidity of the solution may result from the protons evolved in formation of the hydroxy bridge.

For synthesis of **2** and **3**, the pH of the solution is about 4.5. Changing the molar ratio of H_3pdc and the base to 1 : 1 didn't give the desirable product, but 1 : 3 afforded the same product.

Table 2. Selected bond lengths (Å) and angles (°) for **1**.

V(1)–O(5)	1.909(2)	V(1)–O(1)	2.024(2)
V(1)–O(3)#1	1.978(2)	V(1)–O(5)#2	2.038(2)
V(1)–O(6)	2.016(2)	V(1)–N(1)	2.123(2)
O(5)–V(1)–O(3)#1	100.46(7)	O(3)#1–V(1)–O(5)#2	89.74(6)
O(5)–V(1)–O(6)	101.09(7)	O(6)–V(1)–O(5)#2	177.80(7)
O(3)#1–V(1)–O(6)	88.63(7)	O(1)–V(1)–O(5)#2	86.39(6)
O(5)–V(1)–O(1)	160.33(6)	O(5)–V(1)–N(1)	92.61(6)
O(3)#1–V(1)–O(1)	90.94(6)	O(3)#1–V(1)–N(1)	166.89(7)
O(6)–V(1)–O(1)	95.12(7)	O(6)–V(1)–N(1)	87.91(7)
O(5)–V(1)–O(5)#2	77.76(7)	O(1)–V(1)–N(1)	76.79(6)
O(5)#2–V(1)–N(1)	94.00(6)		

Symmetry codes for **1**: #1: $x, y, z-1$; #2: $-x+1, -y+1, -z+1$.

Table 3. Selected bond lengths (Å) and angles (°) for **2**.

V(1)–O(1)	1.617(2)	Na(1)–O(4)	2.319(2)
V(1)–N(2)	2.017(2)	Na(1)–O(3)#3	2.388(2)
V(1)–N(1)#1	2.020(2)	Na(1)–O(5)#4	2.393(2)
V(1)–O(5)#1	2.034(2)	Na(1)–O(6)	2.438(2)
V(1)–O(2)	2.046(2)	Na(1)–O(6)#5	2.600(3)
V(1)–O(1)#2	2.175(2)	Na(1)–O(4)#2	2.633(2)
O(1)–V(1)–N(2)	100.74(8)	N(1)#1–V(1)–O(2)	158.80(8)
O(1)–V(1)–N(1)#1	99.85(8)	O(5)#1–V(1)–O(2)	108.61(7)
N(2)–V(1)–N(1)#1	89.77(8)	O(1)–V(1)–O(1)#2	174.6(1)
O(1)–V(1)–O(5)#1	97.67(7)	N(2)–V(1)–O(1)#2	82.79(7)
N(2)–V(1)–O(5)#1	159.29(8)	N(1)#1–V(1)–O(1)#2	84.13(7)
N(1)#1–V(1)–O(5)#1	77.74(8)	O(5)#1–V(1)–O(1)#2	79.57(6)
O(1)–V(1)–O(2)	99.28(8)	O(2)–V(1)–O(1)#2	77.43(7)
N(2)–V(1)–O(2)	77.73(7)		

Symmetry codes for **2**: #1: $-x, y, -z+1/2$; #2: $x, y+1, z$; #3: $-x, -y+1, -z+1$; #4: $-x-1/2, y+1/2, -z+1/2$; #5: $x, y-1, z$.

Table 4. Selected bond lengths (Å) and angles (°) for **3**.

V(1)–O(1)	1.607(4)	K(1)–O(3)#3	2.775(5)
V(1)–N(1)#1	2.021(5)	K(1)–O(5)#4	2.792(4)
V(1)–O(5)#1	2.025(4)	K(1)–O(4)#5	2.915(5)
V(1)–N(2)	2.026(5)	K(1)–O(2)#6	2.965(4)
V(1)–O(2)	2.027(4)	K(1)–O(3)#6	3.102(5)
V(1)–O(1)#2	2.308(4)	K(1)–O(6)	3.108(3)
K(1)–O(4)	2.751(5)	K(1)–O(4)#4	3.179(5)
O(1)–V(1)–N(1)#1	101.5(2)	O(1)–V(1)–O(2)	101.4(2)
O(1)–V(1)–O(5)#1	101.6(2)	N(1)#1–V(1)–O(2)	155.4(2)
N(1)#1–V(1)–O(5)#1	77.7(2)	O(5)#1–V(1)–O(2)	105.9(2)
O(1)–V(1)–N(2)	101.6(2)	N(2)–V(1)–O(2)	77.7(2)
N(1)#1–V(1)–N(2)	89.3(2)	O(1)–V(1)–O(1)#2	175.8(3)
O(5)#1–V(1)–N(2)	155.3(2)		

Symmetry codes for **3**: #1: $-x+2, y, -z+3/2$; #2: $x, y+1, z$; #3: $-x+2, -y+2, -z+2$; #4: $-x+3, -y+1, -z+2$; #5: $-x+3, -y+2, -z+2$; #6: $-x+2, -y+1, -z+2$.

In the IR spectra, peaks at 858 cm^{-1} for **1**, 855 cm^{-1} for **2** and 859 cm^{-1} for **3** are attributed to ν(V–O) [17]. The strong peaks at 902 cm^{-1} for **2** and 917 cm^{-1} for **3** are assigned to ν(V=O), which are lower than the normal ν(V=O) between 935 and 1035 cm^{-1} [18]. Such a low stretching frequency is associated with the head-to-tail (V=O $\cdots$ V) polymerization [19–21].

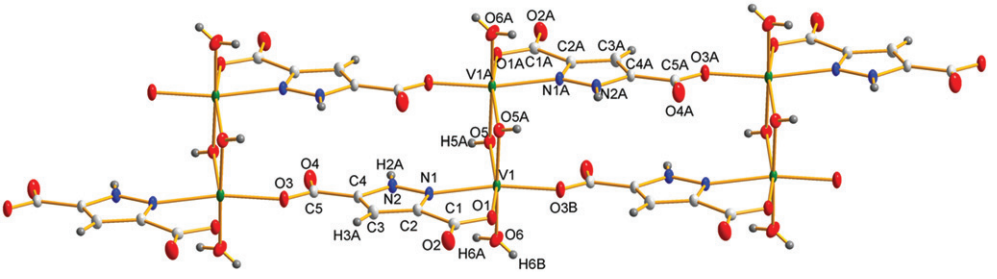

Figure 1. ORTEP drawing (at 50% probability) of **1**.

3.2. *Crystal structure*

3.2.1. $[V_2(\mu\text{-}OH)_2(H_2O)_2(Hpdc)_2]_n$ (1). As shown in figure 1, the structure of **1** consists of infinite double-stranded chains with each V coordinated to two $Hpdc^{2+}$ ligands, two bridging hydroxy groups and a terminal aqua ligand. Neighboring $[VNO_5]$ octahedra share a common edge via the pair of hydroxys with V1–O5–V1A angle of 102.23° and V1–V1A distance of 3.0742 Å. The V–(μ_2–O)(H) bond distances (2.039 and 1.909 Å) are comparable to those of similar bonds [22, 23] and significantly different from the values of V–(μ_2–O) and V–(μ_2–O)(H_2) [24]. The hydroxy groups are derived from water [25, 26]. The double-stranded chains are correlated to form a 3D network through hydrogen bonding. **1** exhibits a gross geometry similar to that of $Ni_2(Hdcp)_2(\mu\text{-}H_2O)_2(H_2O)_2]_\infty$ [15], except that the bridging aqua groups of the Ni complex are replaced by hydroxy groups in **1**.

Since the structure could also have been modeled as $\left[V_2^{IV}(OH)_2(H_2O)_2(pdc)_2\right]_n$, EPR measurement was performed to examine the oxidation state of vanadium; no signal was observed, indicating +3 oxidation state [27]. The BVS calculation [28] of the V ion (3.03) also supports V^{III}.

3.2.2. $\{[Na_2(\mu\text{-}H_2O)_2][V_2O_2(pdc)_2]\}_n$ (2). The structure of **2** is a 3D extended framework. BVS calculation [28] of the V ion (4.06) suggests +4 oxidation state. Each V ion is located at the center of a distorted octahedron with the equatorial plane constructed from two chelating rings of fully deprotonated pdc^{3+} ligands and one axial position occupied by the vanadyl O atom. The pdc^{3+} ligands link two neighboring V ions through pyrazole N–N bridges to form a binuclear subunit with the V–V distance of 4.1323(43)Å (figure 2). The subunits are packed so that the sixth coordination site of the V ion is occupied by the vanadyl O atom from the neighboring subunit, resulting in ladder-like infinite chains along the b axis through V=O–V bonds (figure 3). The chains are further interconnected to one another through pairs of Na^+ chains which also run along b to extend a 3D architecture. Each Na^+ is in a slightly distorted octahedral geometry and coordinated by four carboxylate O atoms from four different pdc^{3+} ligands and two waters. Adjacent Na ions in the pair of chains are connected to one another through bridging carboxylate and water. Although the coordination mode of the pdc^{3+} ligand to the metal ions is close to that of $[\{Na_2(\mu\text{-}H_2O)_2\}\{Cu_2(dcp)_2\}]_\infty$ [15], the distinguishing feature of **2** is that the binuclear subunits of $[V_2O_2(pdc)_2]$ are

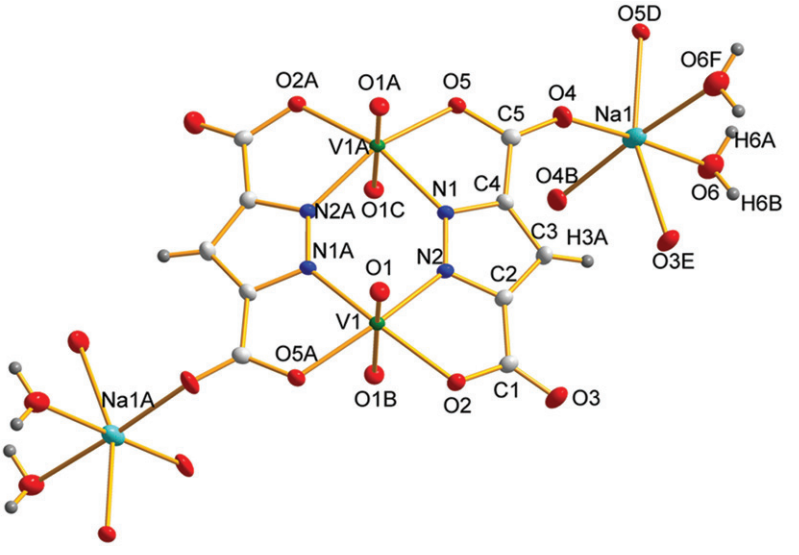

Figure 2. ORTEP representation (at 50% probability) of **2**.

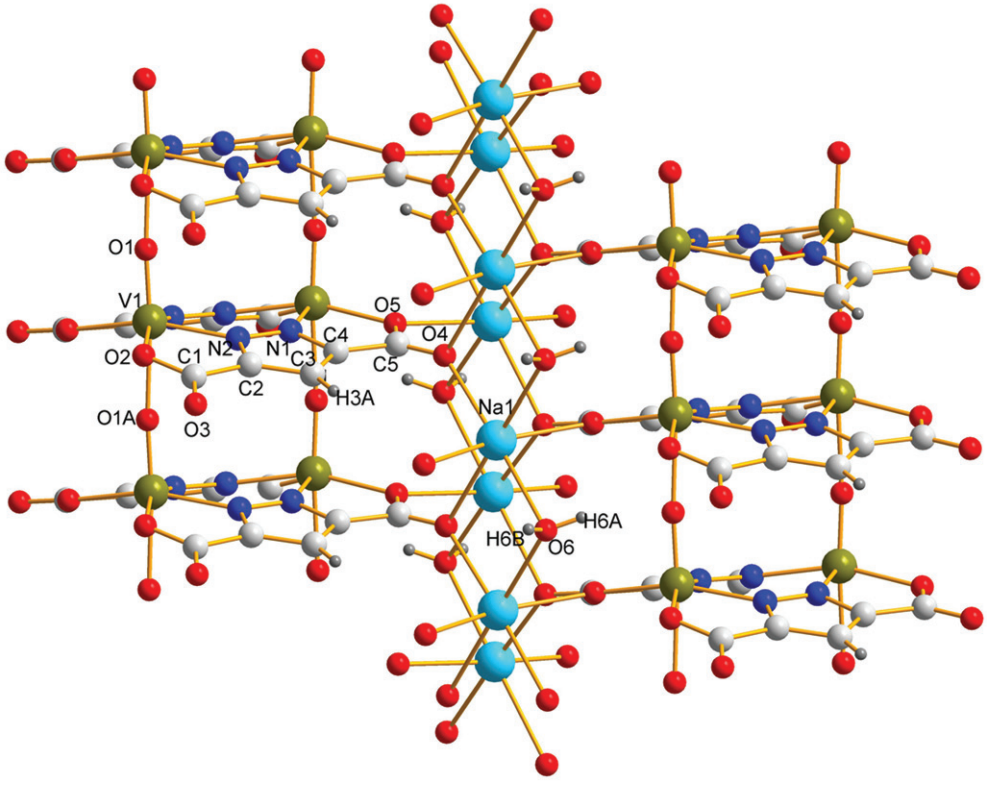

Figure 3. Perspective view of **2** showing the ladder-like infinite chains of V=O–V bonds along the *b* axis.

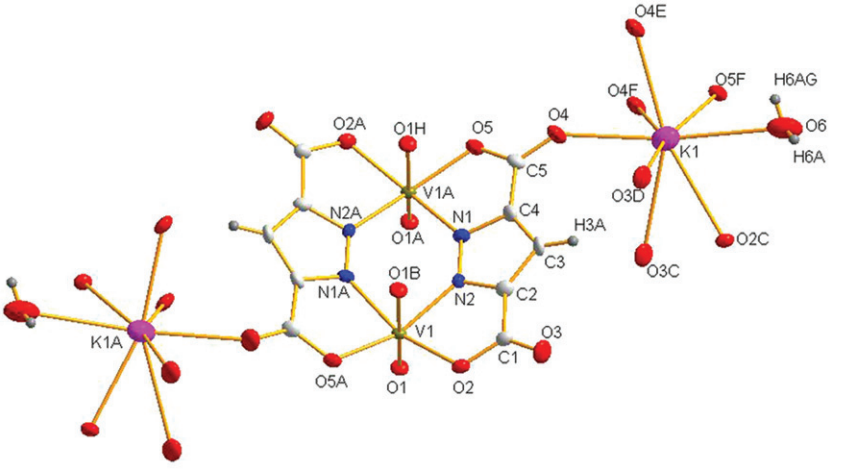

Figure 4. ORTEP representation (at 50% probability) of **3**.

covalently linked by V–O bonds to form ladder-like infinite chains along b, which give rise to different magnetic properties.

Several complexes have been assigned to infinite chains of V=O–V bonds through physical or spectroscopic techniques, but only a few were determined by X-ray crystallography [19, 29–31], most of which are Schiff-base oxovanadium (IV) complexes [29–31]. In addition, few complexes [32] feature ladder-like infinite chains of V=O–V bonds. The angle of V=O–V [174.634(96)°] is quasi-linear, the V–V separation through the oxo bridge is 3.7880(21)Å, and the axial V=O, V–O bond lengths are 1.6175(18)Å and 2.1745(19)Å, respectively, comparable to those of similar bonds in previous reports [19, 29–32]. Both pdc^{3+} ligands of the binuclear subunit tilt toward the b axis to form a dihedral angle of 36.4° between two planes (each defined by four donor atoms of the pdc^{3+} ligand), different from $(VO)_2(pdc)_2$ [10] and $[\{Na_2(\mu\text{-}H_2O)_2\}\{Cu_2(dcp)_2\}]$ [15], in which the eight equatorial donor atoms lie in an approximate plane.

3.2.3. $\{[K_2(\mu\text{-}H_2O)][V_2O_2(pdc)_2]\}_n$ (3). The structure of **3** is similar to that of **2**, also described as ladder-like moieties interconnected by pairs of K ion chains (figures 4–6). The distance between the V ions in the chains along the b axis and the coordination mode of the alkali ions are different from those of **2**. The BVS calculation [28] of the V ion in **3** (4.02) also suggests +4 oxidation state. The V–V distance is 3.9121(17)Å, a little longer than that of **2** (3.7880(21)Å), with the axial V=O, V–O bond lengths of 1.6064(41)Å and 2.3086(41)Å, respectively. Each K^+ is eight-coordinate by seven oxygen atoms from five different carboxylate groups and one water. The K^+ are connected to each other along b by carboxylate O atoms and along the ac plane by water and carboxylate alternately.

3.3. *Magnetism*

Figure 7 shows the plot of χ_m and $\chi_m T$ *versus* T for **1**. The χ_m value increases with decreasing temperature, reaching a maximum at 7 K, and then decreases sharply.

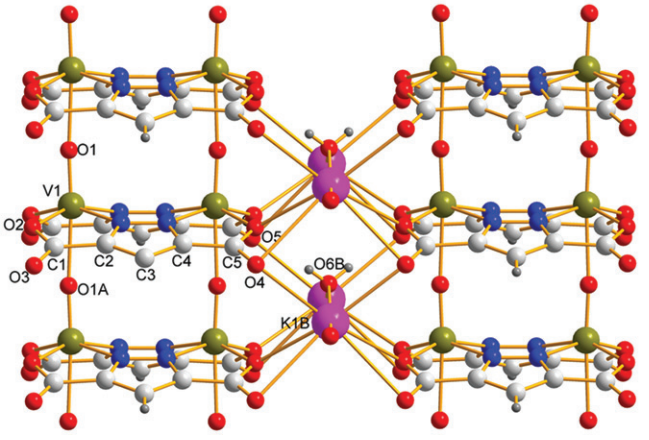

Figure 5. Perspective view of **3** showing the ladder-like infinite chains of V=O–V bonds along the *b* axis.

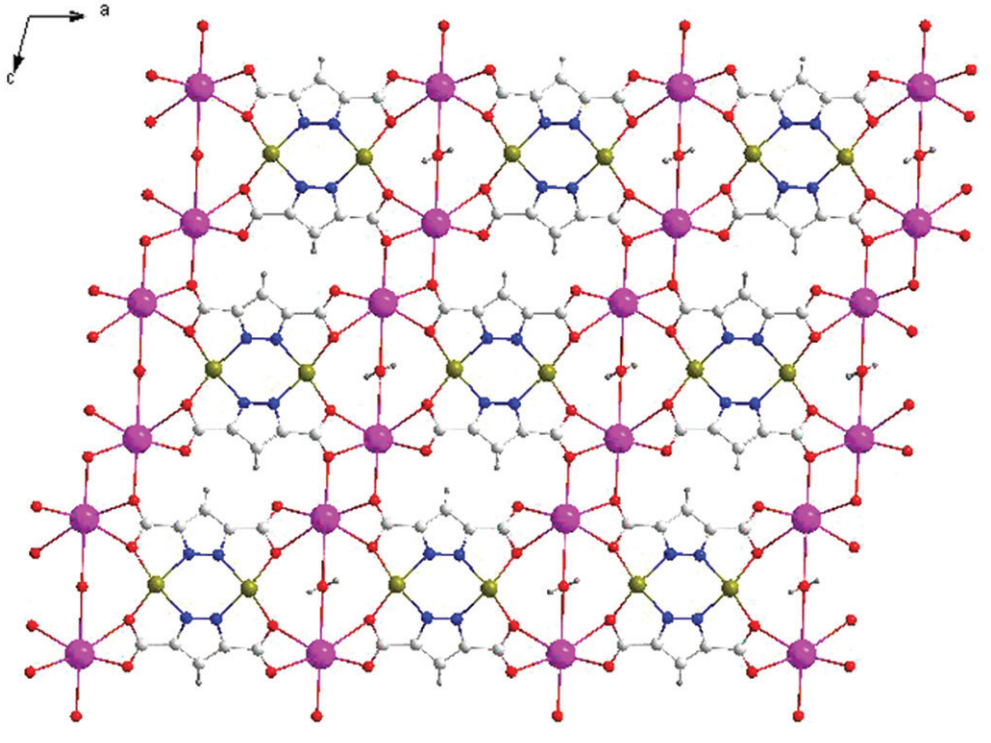

Figure 6. The molecular packing diagram of **3** down the crystallographic *b* axis.

The value of $\chi_m T$ is 1.81 $cm^3 K mol^{-1}$ per V2 unit at room temperature, lower than the spin-only value of 2 $cm^3 K mol^{-1}$ for two uncoupled $S = 1$ vanadium(III) ions. As the distance between the adjacent V ions bridged by $Hpdc^{2+}$ is too large for magnetic coupling, the interactions through them can be neglected. Thus only the interactions through hydroxy bridges were taken into account with an anisotropic

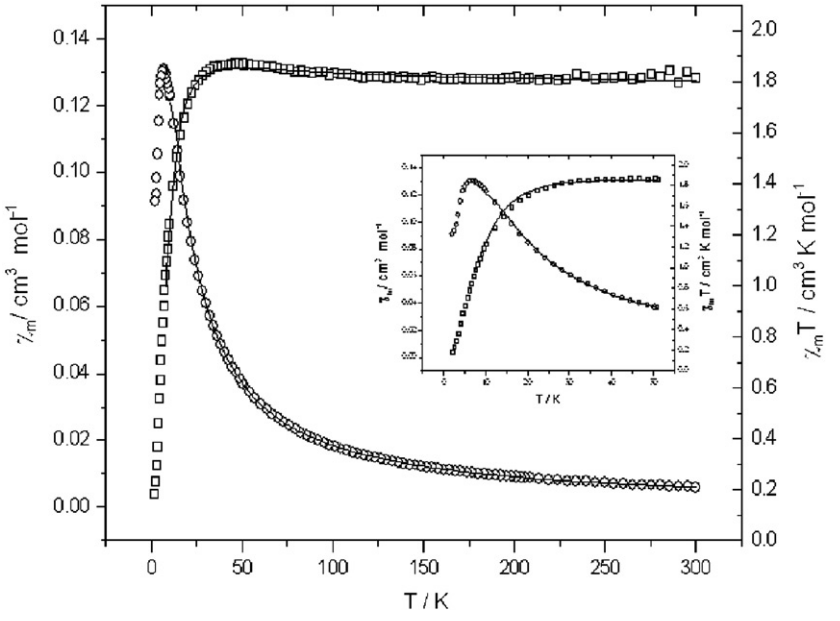

Figure 7. Plot of χ_m (left, circle) and $\chi_m T$ (right, square) *vs.* T per V2 unit for **1**; the solid lines represent the best-fit curves.

Heisenberg $S=1$ dimer model [33] ($H=-2JS_1S_2+D(S_{1z}^2+S_{2z}^2)$) applied to evaluate the magnetic behavior. The data could be fitted from 300–10 K and the best least-square fitting gives $g=1.89$, $J=-2.04\,\mathrm{cm}^{-1}$, $|D|=16.41\,\mathrm{cm}^{-1}$, with an agreement factor of $R=1.4\times10^{-4}$ ($R=\sum[(\chi_mT)_{cal}-(\chi_mT)_{obsd}]^2/\sum[(\chi_mT)_{obsd}]^2$). The results indicate weak antiferromagnetic interactions between neighboring vanadium(III) ions through hydroxy bridges.

Figure 8 shows the plot of χ_m and χ_mT *versus* T for **2**. The χ_mT value at room temperature of $0.7505\,\mathrm{cm}^3\,\mathrm{K\,mol}^{-1}$ per V2 unit is very close to the spin-only value of $0.75\,\mathrm{cm}^3\,\mathrm{K\,mol}^{-1}$ for two uncoupled $S=1/2$ vanadium(IV) ions. As the temperature is lowered, χ_mT increases, indicating dominant ferromagnetic interactions. Below 3.5 K, χ_mT decreases sharply, caused by weaker intermolecular antiferromagnetic interactions.

As described above, the 3D structure of **2** can be viewed as ladder-like moieties, made up of $[V_2O_2(pdc)_2]$ subunits, interconnected by pairs of Na^+ chains. Thus three kinds of magnetic interactions are suggested for the system, namely (i) interactions along the rungs through V–N–N–V linkage; (ii) interactions along the chains through V–O–V linkage; (iii) interchain interactions through carboxylate bridges and Na^+. It is obvious that (iii) is much weaker than (i) and (ii). Therefore, the modified Fisher model for classical spin chain system [34] was applied to evaluate the magnetic behavior. The interactions of (iii) were accounted for by the addition of a mean field term. The Hamiltonian for the 1D chain can be written as $H_{chain}=-J\sum S_{eff,\,i}\cdot S_{eff,\,i+1}$, where S_{eff} represents the effective spin of the binuclear subunit.

The best least-square fitting of the experimental data gives $g=1.95$, $J_1=-1.95\,\mathrm{cm}^{-1}$, $J_2=7.83\,\mathrm{cm}^{-1}$ and $ZJ'=-0.15\,\mathrm{cm}^{-1}$, with an agreement factor of $R=2.5\times10^{-4}$ ($R=\sum[(\chi_mT)_{cal}-(\chi_mT)_{obsd}]^2/\sum[(\chi_mT)_{obsd}]^2$), where J_1 is the spin-exchange parameter for the interaction along the rung, J_2 is the spin-exchange parameter for

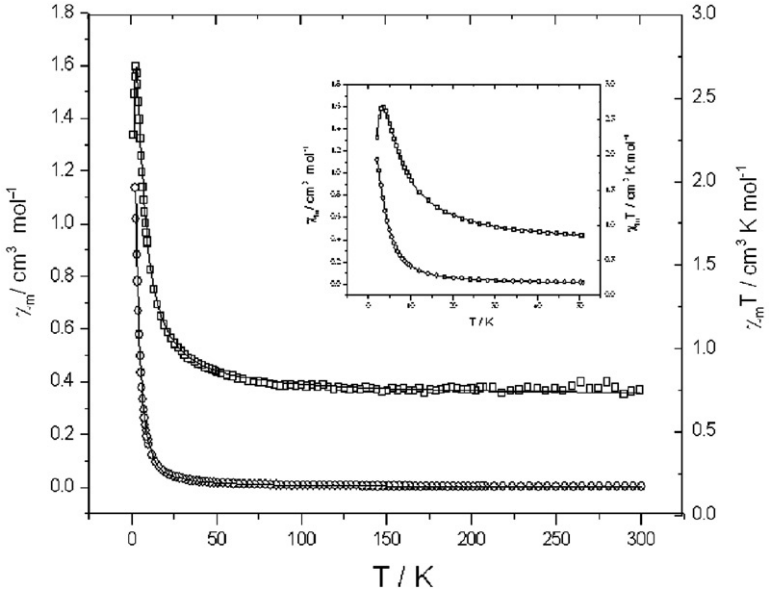

Figure 8. Plot of χ_m (left, circle) and $\chi_m T$ (right, square) *vs.* T per V2 unit for **2**; the solid lines represent the best-fit curves.

the interaction along the chain, J' is the interchain coupling constant and Z is the number of interacting neighbors. The g value is in good agreement with that obtained from EPR ($g = 1.96$). The small negative J_1 value indicates that coupling between V(IV) ions through pyrazole N–N bridge is weakly antiferromagnetic and the positive J_2 value implies ferromagnetic interactions between V ions through oxo bridges along the chain. The small value of ZJ' shows that the interactions through carboxylate bridges and Na ion are very weak.

The plot of χ_m and $\chi_m T$ *versus* T for **3** are shown in figure 9. The $\chi_m T$ value at room temperature is $0.7081\,\mathrm{cm^3\,K\,mol^{-1}}$ per V2 unit. As the temperature is lowered, $\chi_m T$ increases, indicating dominant ferromagnetic interactions. The similar magnetic behavior of **3** to **2** can be expected from their similar structures. The modified Fisher model for classical spin chain system [34] was applied to evaluate the magnetic behavior with g fixed at 1.96, as confirmed by EPR. The best least-square fitting of the experimental data gives $J_1 = -1.55\,\mathrm{cm^{-1}}$ and $J_2 = 4.25\,\mathrm{cm^{-1}}$, with an agreement factor of $R = 2.2 \times 10^{-4}$ ($R = \sum[(\chi_m T)_{cal} - (\chi_m T)_{obsd}]^2 / \sum[(\chi_m T)_{obsd}]^2$). Compared to **2**, the lower value of J_2 is in accord with the longer distance between V^{4+} ions through oxo bridges.

4. Conclusion

We have prepared and characterized three vanadium polymers. BVS calculations, EPR spectra and magnetic data all indicate that vanadium ions are trivalent in **1** and tetravalent in **2** and **3**. The structure of **1** consists of infinite double-stranded chains connected through hydrogen bonds to form a 3D network. Both **2** and **3** exhibit

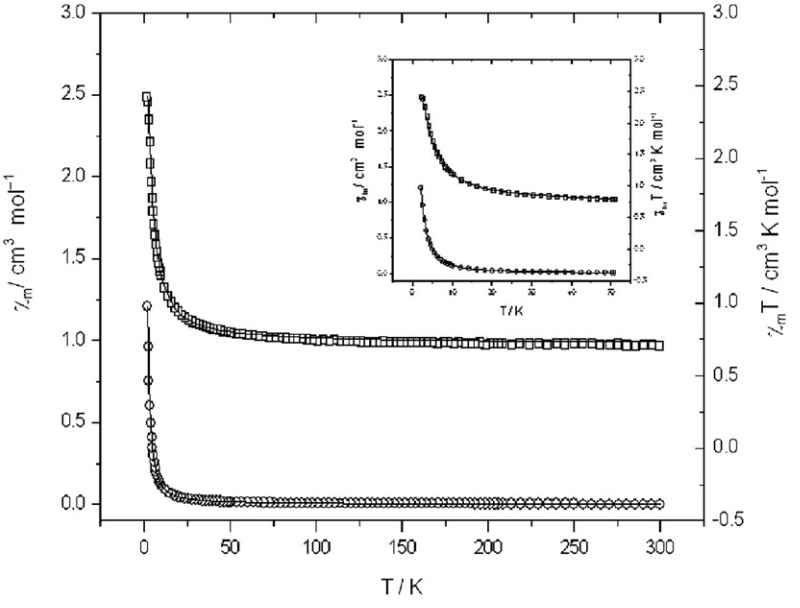

Figure 9. Plot of χ_m (left, circle) and $\chi_m T$ (right, square) *vs.* T per V2 unit for **3**; the solid lines represent the best-fit curves.

a 3D framework which features ladder-like infinite moieties interconnected by pairs of alkali ion chains. The magnetic study of **1** indicates weak antiferromagnetic interactions between neighboring V ions through hydroxy bridges. The magnetic behavior of **2** and **3** reveals dominant ferromagnetic interactions and the least-square fit of the magnetic data indicates ferromagnetic coupling between V ions through oxo bridges along the chain and antiferromagnetic coupling between V ions through pyrazole N–N bridges along the rung.

Supplementary material

EPR spectra and CIF files for **1**–**3**. CCDC 647733, 647734 and 668586 contain the supplementary crystallographic data of the complexes for this article. These data can be obtained free of charge at www.ccdc.cam.ac.uk/conts/retrieving.html [or from the Cambridge Crystallographic Data Centre, 12 Union Road, Cambridge CB2 1EZ, UK. Fax: (internat.) +44-1223/336-033; Email: deposit@ccdc.cam.ac.uk].

Acknowledgements

We are grateful to the National Key Foundation of China (No. 20633020) and the Science & Technology Innovation Foundation of Fujian Province (No. 2007F3112) for financial support of this work.

References

[1] O. Kahn. *Molecular Magnetism*, VCH, New York (1993).
[2] M. Fujita, Y.J. Kwon, S. Washizu, K. Ogura. *J. Am. Chem. Soc.*, **116**, 1151 (1994).
[3] L. Pan, H.M. Liu, X.G. Lei, X.Y. Huang, D.H. Olson, N.J. Turro, J. Li. *Angew. Chem. Int. Ed.*, **42**, 542 (2003).
[4] K. Uemura, S. Kitagawa, M. Kondo, K. Fukui, R. Kitaura, H.C. Chang, T. Mizutani. *Chem. Eur. J.*, **8**, 3586 (2002).
[5] D.N. Dybtsev, H. Chun, S.H. Yoon, D. Kim, K. Kim. *J. Am. Chem. Soc.*, **126**, 32 (2004).
[6] O.R. Evans, W. Lin. *Acc. Chem. Res.*, **35**, 511 (2002).
[7] M. Albrecht, M. Lutz, A.L. Spek, G.V. Koten. *Nature*, **406**, 970 (2000).
[8] J.C. Bayoii, P. Esteban, G. Net, P.G. Ramussen, K.N. Baker, C.W. Hahn, M.M. Gumz. *Inorg. Chem.*, **30**, 2572 (1991).
[9] J.C. Bayoii, G. Net, P. Esteban, P.G. Ramussen, D.F. Bergstrom. *Inorg. Chem.*, **30**, 4771 (1991).
[10] C.W. Hahn, P.G. Rasmussen, J.C. Bayön. *Inorg. Chem.*, **31**, 1963 (1992).
[11] L. Pan, N. Ching, X. Huang, J. Li. *Chem. Eur. J.*, **7**, 4431 (2001).
[12] P. King, R. Clérac, C.E. Anson, C. Coulon, A.K. Powell. *Inorg. Chem.*, **42**, 3492 (2003).
[13] J.L. Tian, S.P. Yan, D.Z. Liao, Z.H. Jiang, P. Cheng. *Inorg. Chem. Commun.*, **6**, 1025 (2003).
[14] S. Baitalik, P. Bag, U. Flörke, K. Nag. *Inorg. Chim. Acta*, **357**, 699 (2004).
[15] P. King, R. Clérac, C.E. Anson, A.K. Powell. *Dalton Trans.*, **6**, 852 (2004).
[16] G.M. Sheldrick. *SHELXTL, Version 5.10.*, *Siemens Analytical X-ray Instruments Inc.*, Madison, Wisconsin, USA (1997).
[17] M.R. Maurya, S. Khurana, C. Schulzke, D. Rehder. *Eur. J. Inorg. Chem.*, **3**, 779 (2001).
[18] J. Selbin. *Chem. Rev.*, **65**, 153 (1965).
[19] M. Mohan, M.R. Bond, T. Otieno, C.J. Carrano. *Inorg. Chem.*, **34**, 1233 (1995).
[20] M. Mathew, A.J. Carty, G.J. Palenik. *J. Am. Chem. Soc.*, **92**, 3197 (1970).
[21] B.J. McCormick, R.A. Bozis. *Inorg. Chem.*, **10**, 2806 (1971).
[22] G. Paul, A. Choudhury, R. Nagarajan, C.N.R. Rao. *Inorg. Chem.*, **42**, 2004 (2003).
[23] M.I. Khan, S. Cevik, D. Powell, S. Li, C.J. O'Connor. *Inorg. Chem.*, **37**, 81 (1998).
[24] M.I. Khan, Y.D. Chang, Q. Chen, J. Salta, Y.S. Lee, C.J. O'Connor, J. Zubieta. *Inorg. Chem.*, **33**, 6340 (1994).
[25] C.R. Cornman, K.M. Geiser-Bush, J.W. Kampf. *Inorg. Chem.*, **38**, 4303 (1999).
[26] T.K. Paine, T. Weyhermüller, L.D. Slep, F. Neese, E. Bill, E. Bothe, K. Wieghardt, P. Chaudhuri. *Inorg. Chem.*, **43**, 7324 (2004).
[27] H. Kumagai, S. Kitagawa, M. Maekawa, S. Kawata, H. Kiso, M. Munakata. *Dalton Trans.*, **11**, 2390 (2002).
[28] W. Liu, H.H. Thorp. *Inorg. Chem.*, **32**, 4102 (1993).
[29] A. Serrette, P.J. Carroll, T.M. Swager. *J. Am. Chem. Soc.*, **114**, 1887 (1992).
[30] S.A. Fairhurst, D.L. Hughes, U. Kleinkes, G.J. Leigh, J.R. Sanders, J. Weisner. *Dalton Trans.*, **3**, 321 (1995).
[31] K. Nakajima, M. Kojima, S. Azuma, R. Kasahara, M. Tsuchimoto, Y. Kubozono, H. Maeda, S. Kashino, S. Ohba, Y. Yoshikawa, J. Fujita. *Bull. Chem. Soc. Jpn*, **69**, 3207 (1996).
[32] H.J. Koo, M.H. Whangbo, P.D. Vernooy, C.C. Torardi, W.J. Marshall. *Inorg. Chem.*, **41**, 4664 (2002).
[33] A.P. Ginberg, R.L. Martin, R.W. Brookes, R.C. Sherwood. *Inorg. Chem.*, **11**, 2884 (1972).
[34] M.E. Fisher. *Am. J. Phys.*, **32**, 343 (1964).